PERGAMON

Journal of Atmospheric and Solar-Terrestrial Physics 61 (1999) 1131–1142

Journal of ATMOSPHERIC AND SOLAR-TERRESTRIAL PHYSICS

First results on daytime mesopause OH rotational temperatures using ground-based photometry from equatorial latitudes

R. Sridharan[a,*], Alok Taori[a], S. Gurubaran[b], R. Rajaram[b], M.G. Shepherd[c]

[a]*Physical Research Laboratory, Ahmedabad 380 009, India*
[b]*EGRL, Indian Institute of Geomagnetism, Tirunelveli 627 001, India*
[c]*York University, North York, Toronto, Canada, M3J 1P3*

Received 11 August 1998; received in revised form 12 August 1999; accepted 13 August 1999

Abstract

Daytime mesospheric OH (8,3) rotational temperatures were estimated from the measurements of the relative intensities of the rotational lines in the same vibrational band, using the unique multiwavelength daytime photometer, from Tirunelveli (8.7°N; 77.8°E; 0.5°N dip latitude), an equatorial station in the Indian zone. On a couple of days when simultaneous measurements were available in the vicinity of the experimental site, the estimated temperatures compared well with those measured by the Wind Imaging Interferometer (WINDII) onboard the Upper Atmosphere Research Satellite (UARS). These results, the first of their kind, revealed: (1) large day-to-day variabilities; (2) oscillatory features with periodicities ranging from 0.5 to 6 h; and (3) large deviations of ±30–50 K, on occasions, from the MSIS-90 model temperatures. Comparisons have also been made with simultaneous measurements of neutral winds around mesopause altitudes using the Partial Reflection radar from the same site to look for any possible association of neutral dynamical parameters with the mesopause temperature variabilities. These results are presented and discussed. © 1999 Elsevier Science Ltd. All rights reserved.

1. Introduction

The mesopause region centered around 85 km and coincident with the region of minimum of the temperature profile acts as an interface between the dense lower atmosphere, i.e. the mesosphere, and the upper atmosphere, namely the lower thermosphere. It also represents the transition zone between those regions dominated by photochemical processes (lower atmosphere) and transport processes (upper atmosphere). While turbulent mixing dominates the lower region ensuring uniform composition, the atmospheric composition is in diffusive equilibrium above 110 km altitude. In short, the mesopause region is said to set the lower boundary condition to the thermosphere above. One of the manifestations of this sort of transitional character is the multiple airglow emitting layers situated close to one another. The three most important airglow emissions from the mesosphere are: (1) vibrational rotational bands of the hydroxyl radical (OH); (2) atomic and molecular oxygen emissions; and (3) emissions from metallic atoms like sodium, magnesium, etc. The main energy source is the solar UV

* Corresponding author. Tel.: +91-1079-462-129; fax: +91-1079-656-0502.

E-mail addresses: sridhar@prl.ernet.in (R. Sridharan), alok@prl.ernet.in (A. Taori), egrl@md3.vsnl.net.in (S. Gurubaran), marianna@windii.yorku.ca (M.G. Shepherd).

PII: S1364-6826(99)00062-0

radiation which dissociates the molecular oxygen into atomic oxygen, which in turn is chemically active. Transport effects enable the downward flux of O towards the mesopause where O_3, OH and active states of O_2 are formed. Excellent reviews on the photochemical processes in the mesopause region are available in the literature (Meriwether, 1989; Sivjee, 1992; and references cited therein).

The mesopause region is also known to act as a filter to many of the upward propagating wave phenomena which are generated in the lower atmosphere, thus acting as a moderator/controller of the coupling between the lower and upper atmosphere. Photochemical processes still dominate this region and determine the overall heat budget. Since most of the chemical reactions are sensitive functions of the ambient temperature, a precise knowledge of the mesopause temperature and its variabilities along with the controlling factors is absolutely essential. Gravity waves and tidal forcings do have significant effects in the mesospheric processes and they modulate the mesospheric temperatures too. Therefore, by monitoring the mesospheric temperatures and their fluctuations which may be of the order of a few degrees in magnitude, with periodicities ranging from a few minutes to several hours, one would be able to investigate mesospheric dynamics as well.

When it comes to the measurements, conventional in-situ methods lack the required precision and are unsuitable. Remote sensing methods are simpler and more reliable with the required temporal resolution. In the latter approach, the intensities of chosen visible airglow lines from molecular bands are isolated from the rest, and measured in the relative (not absolute) sense. The observed ratio in the intensities is known to be a measure of the neutral temperature. Such remote sensing methods could either be attempted from a satellite or by means of ground-based photometers. The former has the advantage of spatial coverage, while the latter provides excellent temporal coverage; the two approaches are mutually complementary. In addition to passive airglow intensity monitoring, sodium Lidars have come to stay with excellent altitude resolution (Fricke and Von Zahn, 1985; Von Zahn et al., 1996). The wide ranging optical methods adopted for remote sensing have been comprehensively reviewed by Meriwether (1984). Emission by the hydroxyl radical (OH) has been widely used for the investigation of the mesopause region. After the discovery of these emissions by Meinel (1950) and a viable and successful explanation of their photochemical origin by Bates and Nicolet (1950), the OH chemistry has been dealt with in considerable detail and these emissions have been widely used for aeronomical studies (Sivjee, 1992, and the references cited therein).

Barring some of the satellite measurements using limb scanning techniques, most of the ground-based measurements are restricted to nighttime, and to moonless periods of the night only. The detection and measurements of rotational line intensities, so as to be able to derive rotational temperatures in the presence of a bright background continuum, has remained a challenge up to this date. With the development of a unique, versatile daytime photometer with multiwavelength capability, measurements of line intensities of chosen rotational lines in the Meinel vibration rotation spectra of the hydroxyl radical (OH), and hence an estimation of rotational temperatures, has become possible. The details of the measurement technique and the first results obtained therein are discussed below.

2. Instrumentation

The multiwavelength daytime photometer (Sridharan et al., 1998) is an advanced version of the single wavelength dayglow photometer (Narayanan et al., 1989; Sridharan et al., 1992). The Dayglow Photometer (DGP) was based on the principle that in the vicinity of the emission feature of interest the background continuum contribution is nearly identical. Two spectral zones, of 0.07 nm typical bandwidth, one containing the emission line along with the background contribution in the same spectral window and the other zone containing only the background, are observed. The wavelength separation between the zones is accomplished by means of a low resolution pressure tuned Fabry–Perot etalon with a narrow band (0.6 nm) prefilter along with a unique discrete mask assembly. These two spectral zones were sampled in quick succession (<10 ms) with the photon intensities counted by means of a synchronous dual counter locked to the respective spectral zones. The difference in the counts counted at a sampling rate of 50 Hz are integrated up to a preset integration period (in this case it is kept at 10 s) and is proportional to the emission line intensity. To change the operating wavelength in the first version of DGP called for changing the instrumental parameters like the tuning condition of the Fabry–Perot etalon, either by changing the pressure or by changing the gap between the etalon plates so as to bring the conditions of central maximum for the wavelength of interest, in addition to changing the prefilter. Near-simultaneous measurements of multiple wavelengths were not possible. These limitations were overcome in a new multiwavelength daytime photometer (MWDPM) by incorporating a spiral mask design (Sridharan et al., 1993). The MWDPM was designed to be able to make measurements at three different wavelengths nearly simultaneously. The broadband FP etalon coated for 400–800 nm with a reflectivity of $\sim$90% forms circular fringes of the chosen wavelengths at the focal plane, where a combination of a spiral mask extending to one free spectral range and a 30° segment mask are mounted concentrically. With one of the masks kept stationary, when the other is rotated the fringe plane is spatially scanned, which means that wavelength scanning with time is accomplished within the free spectral range.

With the rotation of the mask, the spatially separated emission features are displaced in time, making the detection of different wavelength elements straightforward. Initially the photomultiplier is gated for a very short duration which, when translated into wavelength domain, corresponds to a short wavelength interval, of the order of 1/50 of the resultant total spectral width. The gate delay from the reference signal generated from the rotor mask is increased incrementally effecting a gate scanning, which is nothing but the wavelength- or spectral-scanning. After obtaining the profile, the gate width is increased to at least half of the spectral profile and kept fixed with respect to the line centre. The same exercise is carried out for the other wavelengths too. All these gate settings are carried out in the initial setting-up-phase of MWDPM. The region adjoining the line emission is considered to represent the background zone. As in the case of a single wavelength DGP, the photon counts are accumulated for a specified integration time from the regions identified with the signal and the background zones in the independent synchronous counters before the difference representing the intensity of the emission line is deduced. After collecting the data on one wavelength the filter in the front end is changed and the time delays altered accordingly. This operation is repeated for the third filter, thus enabling sampling of the three chosen wavelengths to be done in less than 1 min. The basic design details of electronic gate scanning, performance characteristics, etc., of this fully-automated, computer-controlled, state-of-the-art photometer are available in the literature (Sridharan et al., 1993, 1998). Following the rationale discussed eloquently by Meriwether (1975), the above photometer was operated on two of the chosen rotational lines, namely 731.6 and 740.2 nm, with a filter bandwidth of 0.6 nm each. These two lines are components of the (8,3) vibrational band and they represent the best compromise among (OH) source intensity, the quantum efficiency of the standard photomultiplier tubes and the available interference filters. A Ga–As photocathode photomultiplier which is fairly sensitive in the wavelength region of interest has been used as the detector.

Only relative intensity measurements are made using the MWDPM, though even the long term stability of the instrument is better than the statistical fluctuations. In terms of photon counts, typically the background intensities are of the order of 10^5 counts with the signal intensities forming 7–8% after an integration for 10 s. The instrumental stability is usually ascertained in the laboratory using simulated conditions for nearly the same observing conditions including the intensity levels. Therefore, the statistical fluctuations in the measured photon counts determine the uncertainties in the temperature estimates. The MWDPM is capable of unambiguous detection of line emission intensities which form just 0.05% of the background continuum, while in reality the signal intensities encountered are typically more by two orders of magnitude greater than the detection limit. Extra care has been taken for proper instrument setting for the complete removal of the background continuum as any uncertainty in the intensity estimates of one wavelength would be directly reflected in the derived temperatures. However, once set, the instrumental stability remains good for more than 12 h while the FP etalon pressure tuning may call for a minor adjustment over such long durations.

3. Mesopause rotational temperature estimation

The estimation of rotational temperatures from the relative intensities of the OH rotational lines has been made following the established procedures (Meriwether, 1975, 1984). These vibrationally excited OH molecules become locally thermalized due to their sufficiently long lifetime in the excited state as compared to the intercollisional period (Krassovsky et al., 1977). Therefore, the calculated rotational temperatures are considered as a good measure of the ambient temperature.

If the population of the excited state follows the Maxwell Boltzmann distribution, the relative intensity of the rotational line with wavelength λ and quantum number K can be written as:

$$I(K) = AS(K)\lambda^{-3} \exp\left[-f_v(K)\frac{hc}{kT_r}\right] \tag{1}$$

where $I(K)$ is in photon units for the particular emission line; A is a constant. $S(K)$ is a function proportional to the rotational line strength, and $f_v(K)$ is the rotational term value for the particular vibration level v. T_r is the rotational temperature representing a weighted average of the distribution of temperatures over the OH volume emission rate profile. Following the approach of Meriwether (1975, 1984), $S(K)$ and $F_v(K)$ were obtained from Mies (1974) and the factor hc/k is 1.439 K cm. I_1 and I_2 represent the integrated column emission rates of the selected rotational lines expressed in Rayleighs. When we use only the $P_1(2)$ and $P_2(5)$ lines (i.e. $K = 2$ and 5) of the (8,3) band, with wavelengths 731.6 and 740.2 nm, as in the present case, the expression (Meriwether, 1975, 1984) for the

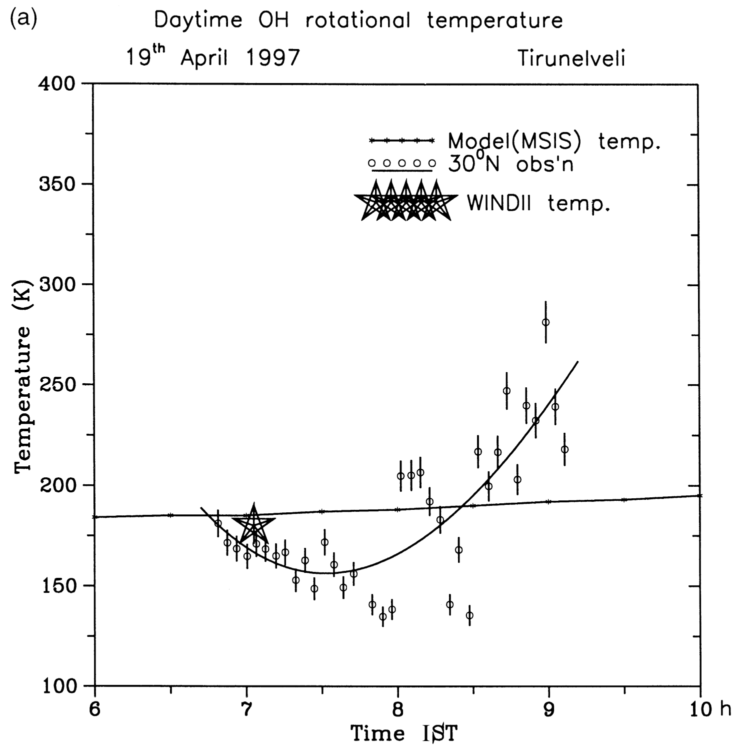

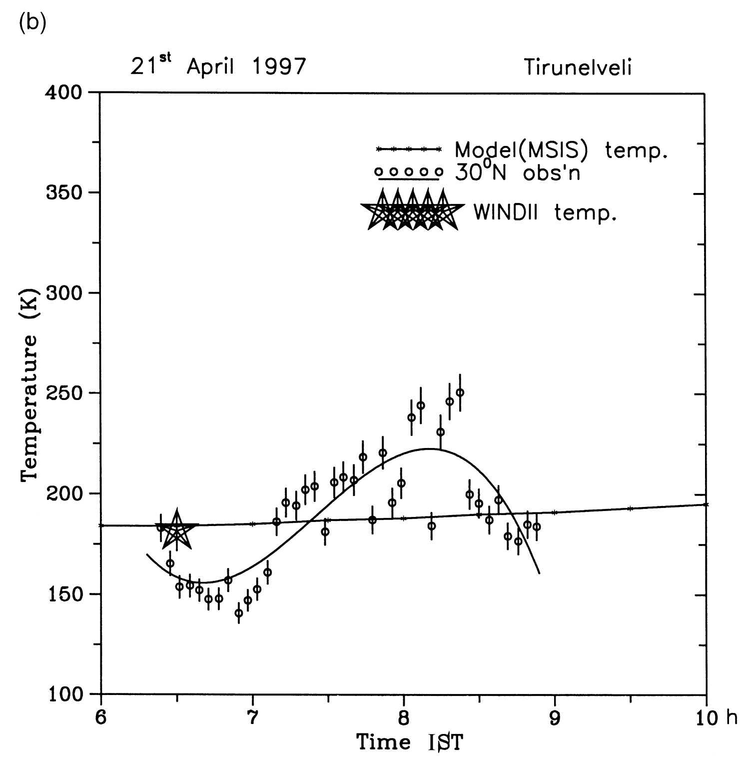

Fig. 1. (a) The variabilities in the mesopause rotational temperatures derived on 19 April 1997 for the equatorial station Tirunelveli. The continuous line depicts the MSIS-90 model prediction, while the 'star' indicates the spot value at 84 km estimated by the WINDII experiment on the UARS satellite. (b) Same as (a), but for 21 April 1997.

rotational temperature takes the form:

$$T_r = \frac{362}{\ln\left(3.44 \times \frac{I_1}{I_2}\right)} \quad (2)$$

4. First results

The MWDPM was operated from Tirunelveli (8.7°N, 77.8°E, 0.5°N dip latitude), a station located very close to the magnetic dip equator. Rotational temperatures were estimated from the relative intensity measurements for about two hours in the mornings of 19 and 21 April 1997. Bad sky conditions prevented continuous operation of the photometer. These results bear special significance as the Upper Atmosphere Research Satellite (UARS) was crossing this zone in the near vicinity, and therefore the ground-based coordinated measurements constitute a unique set. Fig. 1a depicts the estimated temperature variabilities based on raw data along the 30° look angle of the photometer pointing northwards. On 19 April, the observations were started at 06:45 IST. At that time the estimated temperatures were close to the MSIS-90 model (which is a version of MSIS-86 extended by using a lower atmospheric model, namely the CIRA-86 model; Hedin, 1991) predictions for that day. The maximum deviation from the model was as high as 40–50 K. Significant differences were noticed on this day in the variability of the estimated temperatures at different elevations. (For an emission height of 85 km, the look angles when translated into horizontal distances, by calculating the ground projection, turn out to be 20 km between the adjacent angles.) The inferred temperature difference within this short distance needs to be validated with more data as the gate width settings for one direction, even if slightly different from what it should actually be, would reflect in the inferred temperatures. This possibility could not be ruled out as a few more days of data obtained during March 1998 do not show such spatial variabilities (presented and discussed later). The results of 21 April 1997 depicted in Fig. 1b show distinctly different variabilities with regard to the phase of the variations (opposite in phase). The model values remain fairly steady around 188 K. With a maximum deviation of ±50 K from the model, the results from these observations on these two days, though extending to hardly two hours duration on each day, are considered important as nearly simultaneous satellite-based measurements were available, enabling an independent validation of the ground-based optical technique.

5. Validation of the estimated daytime rotational temperature by UARS-WINDII data

The MWDPM is a relative intensity measuring instrument. Though extreme care is taken to remove the background continuum, since the continuum intensities are typically two orders of magnitude larger than the emission line intensities, any imbalance in the continuum rejection in any one of the wavelengths monitored will lead to errors. Therefore, it becomes important to check and validate the method with another independent proven technique. In the present case, comparisons have been made with the UARS-WINDII data as the ground-based measurements were made to coincide with the satellite pass in the near vicinity. The WIND Imaging Interferometer payload onboard the UARS satellite measures 553.0 nm as background for the 557.7 nm O (^{1}S) greenline emission intensities, from the lower thermosphere. For daytime measurements, the observed background in the altitude region of 70 to 110 km is dominated by Rayleigh scattering which is proportional to the total density integrated along the line of sight. These scattered intensities are used to derive a density profile from which the altitude profile of temperature is derived under the hydrostatic equilibrium assumptions (Chanin and Hauchecorne, 1984; Shepherd et al., 1997; Chahine, 1970). A density scale height $H(z)$ is determined for each height z by fitting the intensity $I(z)$ as:

$$\frac{-1}{I(z)}\frac{\mathrm{d}I(z)}{\mathrm{d}z} = H(z) \quad (3)$$

Air pressure $P(z)$, density $n(z)$ and temperature $T(z)$ are related by:

$$P(z) = \frac{Rn(z)T(z)}{m} \quad (4)$$

where m is the mean molecular mass and R is the universal gas constant

$$\mathrm{d}P(z) = -n(z)g(z)\mathrm{d}z \quad (5)$$

so

$$\frac{\mathrm{d}P(z)}{P(z)} = \frac{mg(z)}{RT(z)}\mathrm{d}z = \mathrm{d}[\log\ P(z)] \quad (6)$$

if g and the temperature are assumed to be constant in the ith layer, then the pressure at the bottom and top of the layer are related by:

$$\frac{P(z_i - \Delta z/2)}{P(z_i + \Delta z/2)} = \exp\left[\frac{mg(z_i)}{RT(z_i)}\Delta z\right] \quad (7)$$

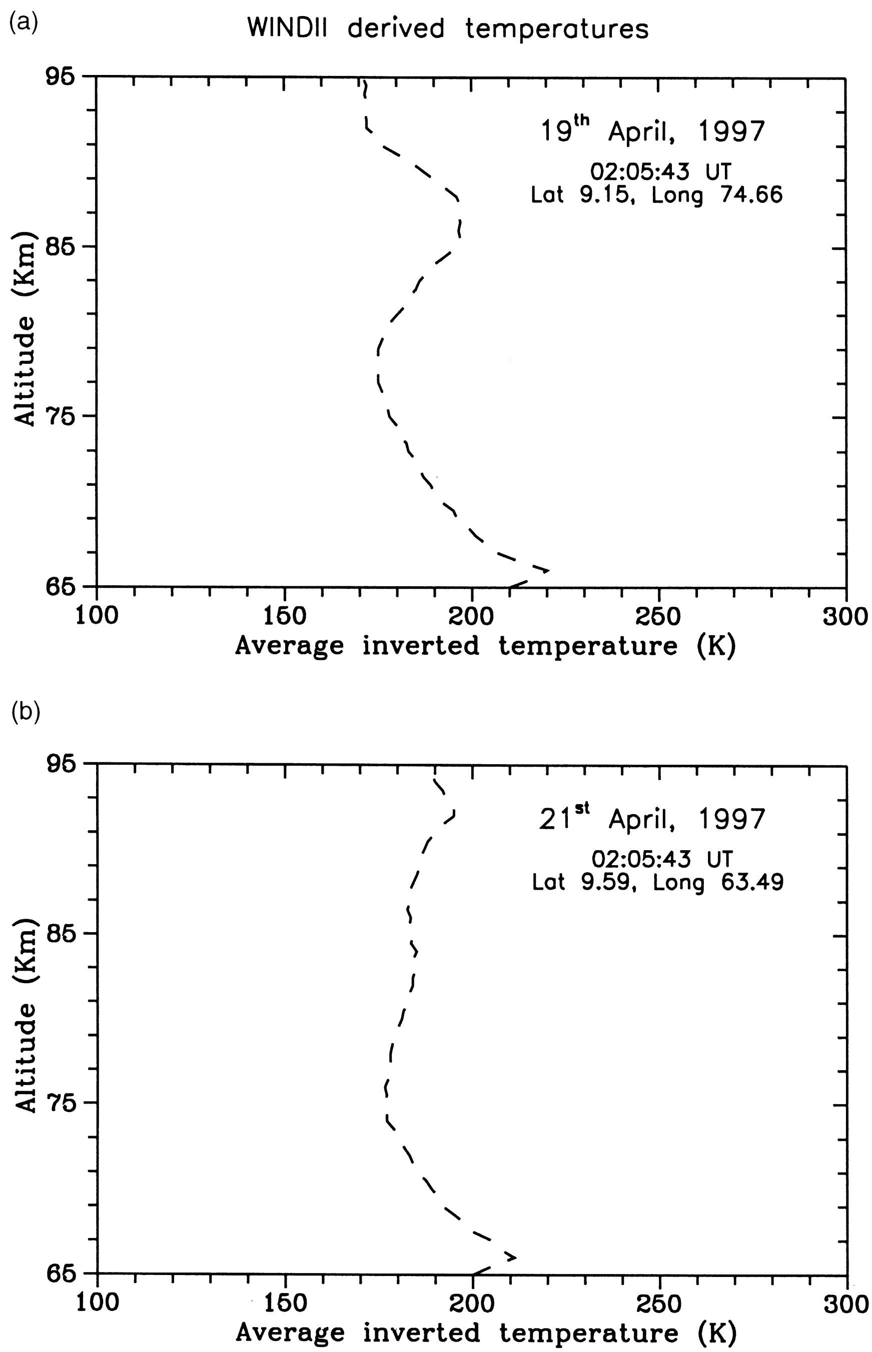

Fig. 2. (a) The altitude profile of the neutral temperature as derived from the Rayleigh scattered intensities monitored by the Wind Imaging Interferometer (WINDII) onboard the UARS satellite on 19 April 1997. (b) Same as (a), but for 21 April 1997.

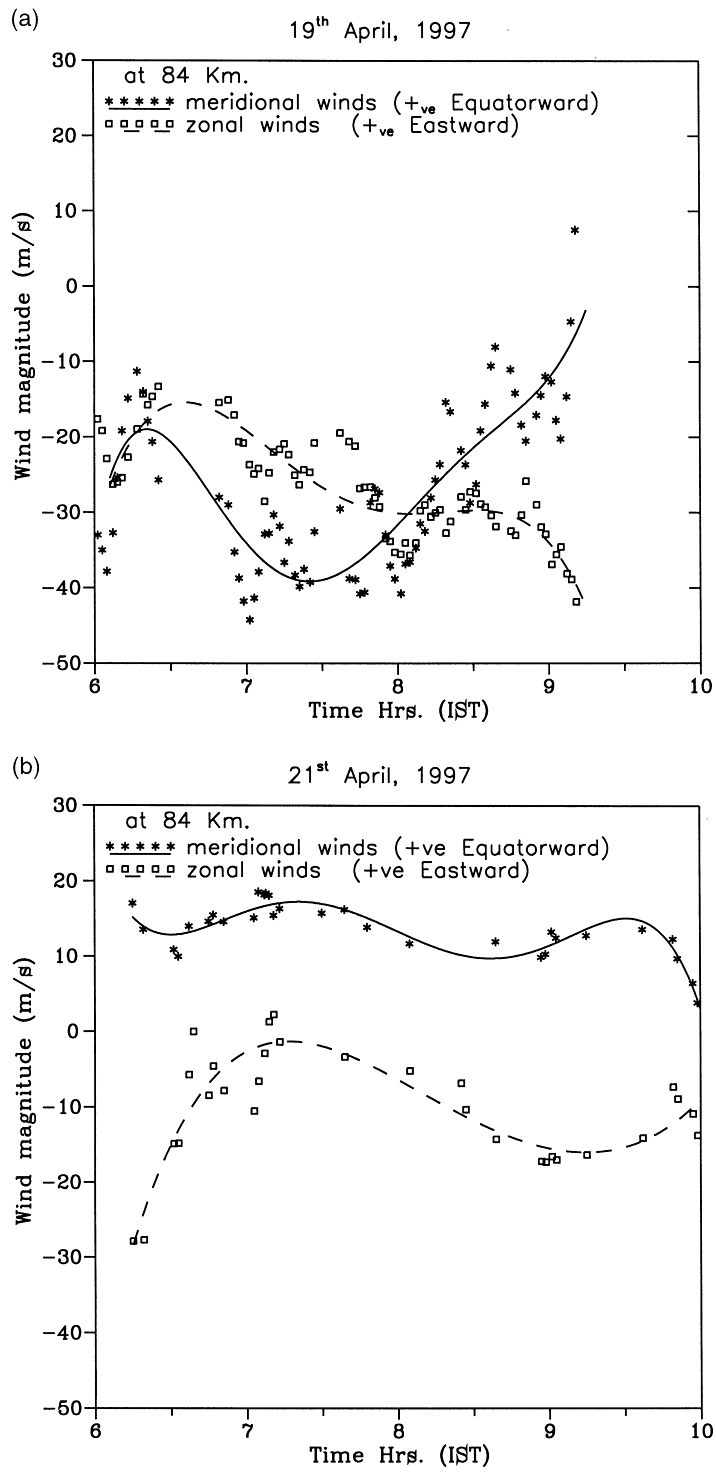

Fig. 3. (a) The temporal variability of the meridional and zonal wind components as obtained by the Partial Reflection radar, operated from Tirunelveli on 19 April 1997. (b) Same as (a), but for 21 April 1997.

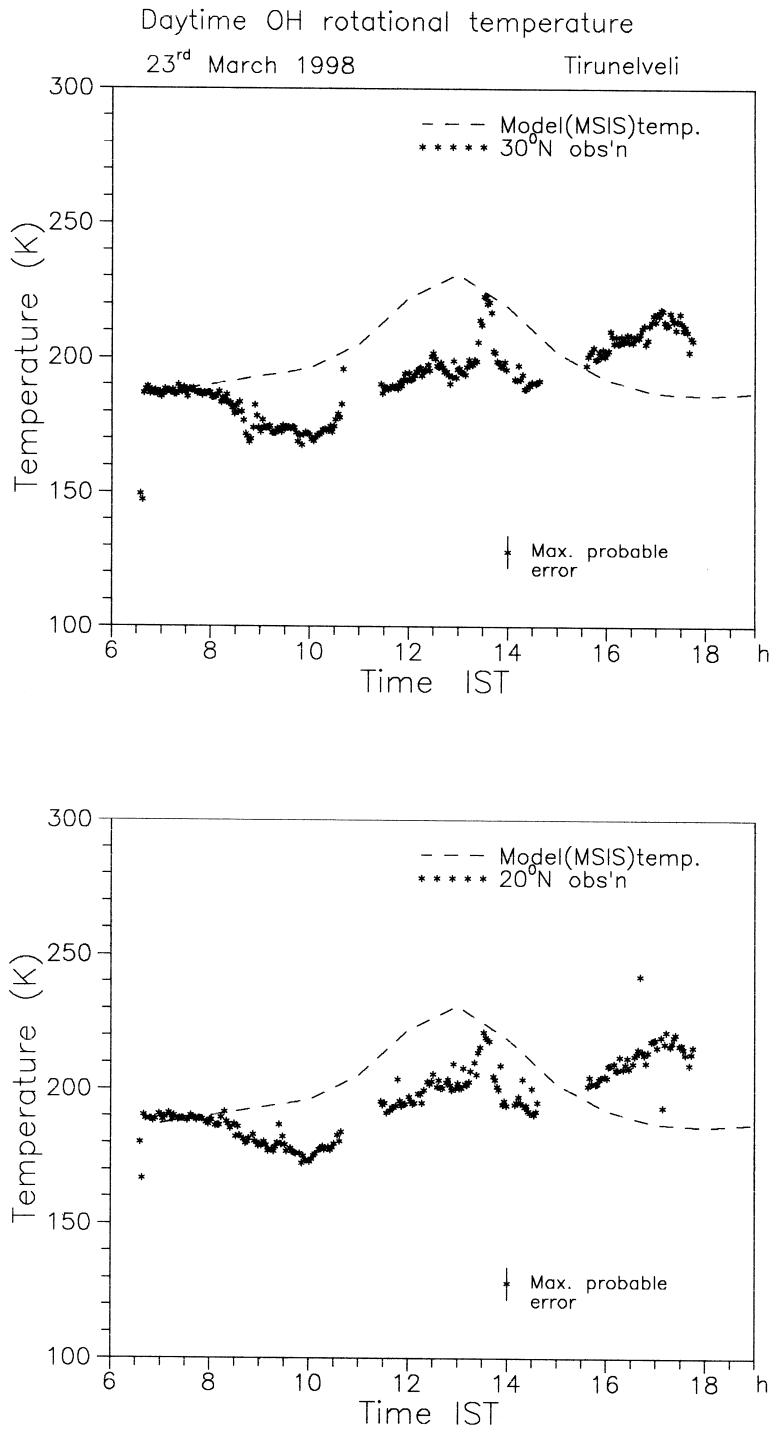

Fig. 4. The rotational temperature variabilities for two look angles, 20 and 30° pointing North on 23 March 1998.

Thus, the temperature is expressed as:

$$T(z_i) = \frac{mg(z_i)\Delta z_i}{R \ \ln\left[\dfrac{P(z_i - \Delta z/2)}{P(z_i + \Delta z/2)}\right]} \tag{8}$$

Density profiles calculated by Eq. (3) are used to obtain pressure values using the MSIS model, and their substitution into Eq. (8) will yield the temperatures (Chanin and Hauchecorne, 1984). One of the assumptions is that the temperature at 110 km is ~230 K for the MSIS-90 model. This assumption and the method of temperature retrieval have been validated by Shepherd et al. (1997) by comparing the same with a variety of ground-based and spaceborne techniques.

The mean temperature profiles obtained for 19 and 21 April 1997 are given in Figs. 2a and 2b, along with the geographic coordinates corresponding to the measurements. While, on 19 April, the latitude is close to that of the ground-based observation, the satellite measurements correspond to ~4° West of the ground site. On 21 April, it was to the West of the observation site, by 15°, though at around the same latitude. One more profile in the same longitude, but at latitudes >20° away in latitude from the observation site, is not presented here as the meridional scan of the optical instrument does not extend this far. The temperatures corresponding to the OH emission height of 85 km as obtained from the WINDII experiment of the UARS satellite is depicted in Figs. 1a and 1b by a star. The uncertainties in the WINDII estimates do not exceed ±5%. These temperature estimates and that from the relative intensities of OH rotational lines appear to be in broad agrement, within the experimental uncertainties.

6. Effects of mesospheric dynamics on daytime rotational temperatures

The partial reflection (PR) radar at 1.98 MHz was operated from Tirunelveli (8.7°N; 77.8°E) from where the ground-based optical measurements were carried out. The PR radar makes use of the spaced antenna technique, and samples the horizontal winds in the 60 to 98 km altitude region. Full correlation analysis (Briggs, 1984) has been carried out to deduce the wind components following standard procedures presented elsewhere (Rajaram and Gurubaran, 1998). In the present study, radar data corresponding to 84 km height

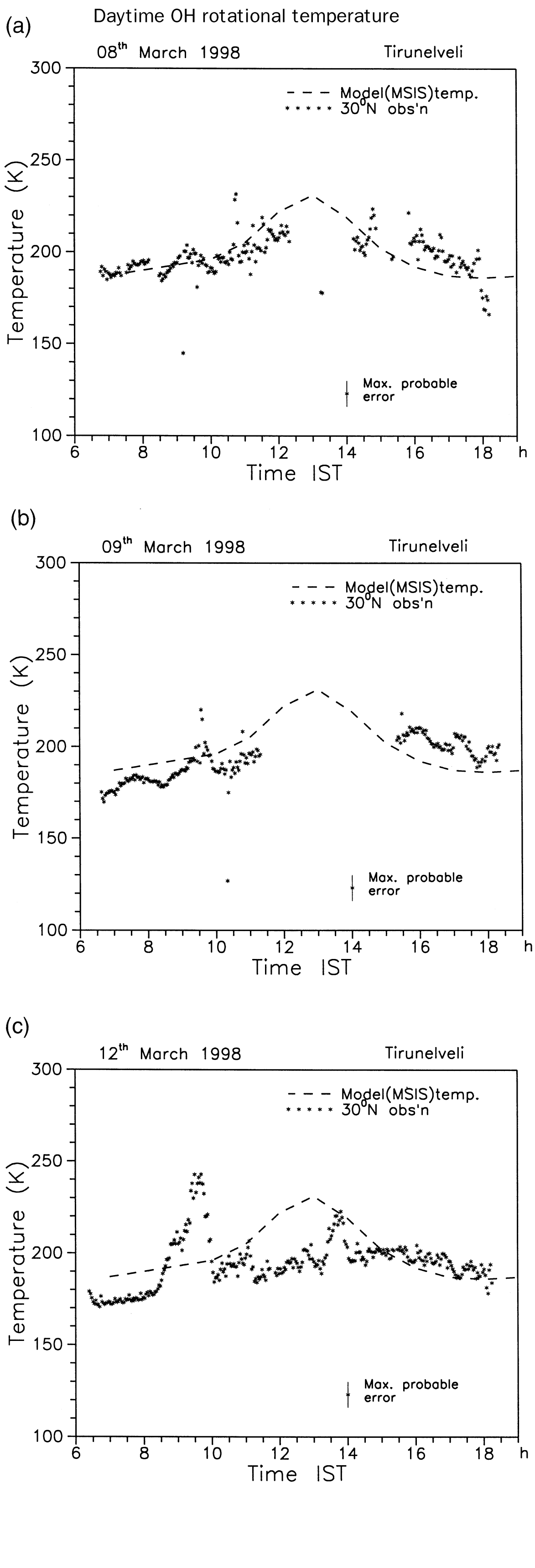

Fig. 5. (a) Same as Fig. 4, but for 8 March 1998, 30° look angle pointing North. (b) Same as Fig. 5a, but for 9 March 1998. (c) Same as Fig. 5a, but for 12 March 1998.

on both 19 and 21 April 1997 are utilized to examine the short period wind fields. Figs. 3a and 3b depict the nature of the variabilities in the wind components on 19 and 21 April. The data points were smoothed by taking a five point running average. Short period, ~45 min fluctuations were quite prominent on 19 April in both the zonal and meridional wind components, while these fluctuations were absent on 21 April. For the present we are considering only the long period variations as depicted by the fifth-order polynomial fit on both days. On 19 April, the meridional wind reached a maximum of ~40 ms^{-1}, at around 0730 IST (Indian Standard Time), and equatorward, while on 21 April it was poleward with a magnitude of ~18 ms^{-1}. It should be noted that the zonal wind magnitude remained close to zero from 07:00 to 08:30 IST on 21 April. It is interesting to note that the variabilities of both the meridional component of the neutral winds and the rotational temperatures were similar, indicating a possible link mainly through wave activity in the mesosphere. More detailed, coordinated measurements are planned in the future to confirm this point.

7. Further results

After having validated the technique of retrieval of the OH rotational temperature, data for a few more days were obtained during March 1998. Four days of data, when extended observations were available, are presented in Figs. 4 and 5. The viewing conditions were unfavourable this year too, due to a continuous overcast sky, and only limited observations could be made. Unfortunately the PR radar had some technical problems during this campaign and no simultaneous wind measurements could be made. In spite of the limited data, large day-to-day variabilities, and periodicities ranging from 0.5 to 6 h, could easily be seen on all the days in the mesopause temperatures. Fig. 4 depicts the inferred mesopause temperatures on 23 March 1998 for two look angles of 20 and 30° elevations pointing North. The data have not been subjected to any smoothing or processing. Unlike the earlier case, the data at both the look angles show identical variations. Though initially up to 08:00 IST the measurements agreed very well with the model, they began to deviate from it and, by 10:00 IST, the difference was as much as 30 K, the observed value being less than the model value. From 10:00 to ~15:00 IST the trends were very similar in both the model and measurements. Beyond 15:00 IST the measurements showed an increasing trend, while the model predicted an asymptotic decrease. One could see a dominant 6 h period in the measurements.

Fig. 5a depicts the temperature data corresponding to 8 March 1998. On this day no data could be collected during 12:00–14:00 IST due to clouds. The measurements were centered with respect to the model values, and the deviation, if any, was only marginal up to 14:00 IST. Beyond 15:00 IST the measurements were higher, by 20 K, and a steep decrease was recorded beyond 17:30 IST.

Fig. 5b depicts the temperature data corresponding to 9 March 1998. On this day too no data could be collected from 11:00 to 15:00 IST due to poor viewing conditions. In the morning hours the measured temperatures turned out to be slightly less than the model values, while in the afternoon they were greater. Very clear oscillatory features with periods ranging from 1 to 1.5 h were present.

The next day when measurements could be made was on 12 March 1998 (Fig. 5c). Unlike the two days considered so far, continuous data could be obtained from the morning 06:30 to 17:45 IST. The measurements were deviating significantly from the model values up to ~14:00 IST. The rotational temperatures registered a steep increase at 08:15 IST, by ~25 K. Small scale fluctuations were recorded all through the day, with periods ranging anywhere from 0.5 to 2 h. The mean of the inferred temperatures was constant at near 185 K.

8. Discussion

The extended data for a few more days during the month of March 1998 brings out clearly the large day-to-day variabilities exhibited by the rotational temperatures. The detected variabilities based on the periodicities indicate that these oscillations could be due to the modulation of the temperature by gravity waves prevalent in these regions. These sorts of wave-like disturbances could originate from below, in the tropospheric and stratospheric regions. It is well known that, as waves propagate upward, they grow in amplitude in order to conserve their energy, due to monotonically decreasing densities. In spite of the stratosphere acting as a filter, for the disturbances originating in the troposphere due to the prevailing conditions, even disturbances of extremely small amplitudes would become large enough to modulate the densities and temperatures at mesospheric altitudes and above. Another possibility is the horizontal propagation of waves near the mesopause region.

Once the mesopause region is shown to be so sensitive and prone to large variabilities, presumably due to neutral dynamical forcings, it becomes extremely important to be able to characterize these variabilities and also identify the possible causative mechanisms. As such, almost all the atmospheric models make an assumption that the mesopause temperature is invariant and our present results therefore have important ramifications.

Further, it is well appreciated that OH emissions are good indicators of the processes in the mesopause region at an altitude ~85 km, with a semi-thickness of ~6 km irrespective of the geographical location (Rogers et al., 1973; McDade et al., 1987; Lopez-Moreno et al., 1987) (though on occasions precise measurements using sodium Lidars have revealed two minima, with the second minima being located around 100 km, Von Zahn, 1996). It was necessary to establish the above points before the relative intensity of rotational lines could be successfully used to determine the nighttime mesopause temperatures (Meriwether, 1975; Takahashi et al., 1994; Sahai et al., 1996). Nocturnal variations with periods from 15 minutes to a few hours over a wide range of latitudes, with large day-to-day variabilities, have been reported in the literature (Meriwether, 1975; Majmudar and Kulkarni, 1979; Cogger et al., 1988; Takahashi et al., 1989; Elphinstone et al., 1988; Swenson et al., 1990; Dewan and Picard, 1998). The spatial and temporal variabilities in the rotational temperatures have been used when deducing the dynamical parameters, such as gravity waves.

The present results are the first of their kind made during daytime conditions. The experimental uncertainties do not exceed ±7.5 K. Often, large variabilities, generally around the MSIS-90 model values, with periodicities ranging from 0.5 to 6 h have been detected. The comparison of the estimated temperatures with UARS data could be treated only as an order of magnitude comparison since the UARS measurements corresponded to geographical locations separated by from 4 to 15° in longitude on 19 and 21 April 1997. In spite of this, the photometric results presented here are of the same magnitude as the values deduced from the WINDII data and, in turn, have been independently validated. The other important result is the similarity in the temporal variability of neutral wind components from the Partial Reflection radar data, which calls for a more detailed study. The MWDPM when operated from a place on the dip equator provides immense opportunities to investigate the coupling processes between the lower and upper atmosphere in the electrojet region. More systematic coordinated measurements, with the Partial Reflection radar providing neutral wind data and the VHF and HF radars yielding the drift velocity of the plasma density irregularities associated with the equatorial electrojet, are planned for the near future.

Acknowledgements

The active participation of Ms R. Narayanan, N. K. Modi and D. Chakrabarty in setting up the experiment in Tirunelveli is duly acknowledged. This work is supported by the Department of Space, Government of India.

References

Bates, D.R., Nicolet, M., 1950. The photochemistry of atmospheric water vapour. Journal of Geophysical Research 55, 301–327.

Briggs, B.H., 1984. The analysis of spaced sensor records by correlation technique. In: MAP Handbook, vol. 13, pp. 166–186.

Chahine, M.T., 1970. Inverse problem in radiative transfer, a determination of atmospheric parameters. Journal of Atmospheric Science 27, 960–967.

Chanin, M.L., Hauchecorne, A., 1984. Lidar studies of the temperature and density using Rayleigh scattering. In: MAP Handbook, vol. 13, pp. 87–99.

Cogger, L.L., Elphinstone, R.D., Giers, D.H., 1988. Wave characteristics obtained from OH rotational temperatures and 557 nm characteristics obtained from OH rotational temperatures and 557.7 nm airglow intensities. Journal of Atmospheric and Terrestrial Physics 50, 943–949.

Dewan, E.M., Picard, R.H., 1998. Mesospheric bores. Journal of Geophysical Research 103, 6295–6305.

Elphinstone, R.D., Cogger, L.L., Murphee, J.S., Murty, G.S.N., Meriwether Jr, J.W., 1988. The analysis of hydroxyl rotational temperatures to characterize moving thermal structure near the mesopause. Journal of Atmospheric and Terrestrial Physics 50, 657–668.

Fricke, K.H., Von Zahn, U., 1985. Mesopause temperatures derived from probing the hyperfine structure of the D2 resonance line of sodium by Lidar. Journal of Atmospheric Terrestrial Physics 47 (5), 499–512.

Hedin, A.E., 1991. Extension of the MSIS thermosphere model into the middle and low atmosphere. Journal of Geophysical Research 96, 1159–1172.

Krassovsky, V.I., Potapov, B.P., Semenov, A.I., Sobolev, V.G., Shagaev, M.V., Shefov, N.N., 1977. On the equilibrium nature of the rotational temperature of hydroxyl airglow. Planetary and Space Science 25, 596–597.

Lopez-Moreno, J.J., Rodrigo, R., Moreno, F., Lopez-Puertas, M., Molina, A., 1987. Altitude distribution of vibrationally excited states of atmospheric hydrodistribution of vibrationally excited states of atmospheric hydroxyl at levels $v=2$ to $v=7$. Planetary and Space Science 35, 1029–1038.

Majmudar, Neeta, Kulkarni, P.V., 1979. Measurements of neutral temperature in 80–90 km region with OH nightglow emission. Indian Journal of Radio and Space Physics, 8, 193–196.

McDade, I.C., Llewellyn, E.J., Murtagh, D.P., Greer, R.G.H., 1987. ETON 5: simultaneous rocket measurements of the OH Meinel $\Delta v=2$ and (8,3) band emission profiles in the nightglow. Planetary and Space Science 35, 1137–1147.

Meinel, A.B., 1950. OH emission bands in the spectrum of the night sky. Astrophysical Journal 111, 555–564.

Meriwether Jr, J.W., 1975. High latitude airglow observations of correlated short term fluctuations in the hydroxyl Meinel 8-3 band intensity and rotational temperature. Planetary and Space Science 23, 1211–1221.

Meriwether Jr, J.W., 1984. Ground based measurements of mesospheric temperatures by optical means. In: Map Handbook, vol. 13, pp. 1–18.

Meriwether Jr, J.W., 1989. A review of the photochemistry of selected nightglow emissions from the mesopause. Journal of Geophysical Research 94 (D12), 14,629–14,646.

Mies, F.H., 1974. Calculated vibrational transition probabilities of OH (X 2π). Journal of Molecular Spectroscopy 53, 150–188.

Narayanan, R., Desai, J.N., Modi, N.K., Raghavarao, R., Sridharan, R., 1989. Dayglow photometry: a new approach. Applied Optics 28, 2138–2142.

Rajaram, R., Gurubaran, S., 1998. Seasonal variabilities of low latitude mesospheric winds. Annales Geophysicae 16, 197–204.

Rogers, J.W., Murphy, R.E., Stair, A.T., Ulwick, J.C., Baker, K.D., Jensen, L.L., 1973. Rocket borne radiometric measurements of OH in the auroral zone. Journal of Geophysical Research 78, 7023–7031.

Sahai, Y., Giers, D.H., Cogger, L.L., Fagundes, P.R., Garbe, G.P., 1996. Solar flux and seasonal variations of the mesopause temperatures at 51°N. Journal of Atmospheric and Terrestrial Physics 58 (16), 1927–1934.

Shepherd, M.G., Dudhia, A., Lopez-Puertas, M., Evans, W.F.J., 1997. Upper mesospheric temperatures in summer: WINDII observations and comparisons. Geophysical Research Letters 24, 357–360.

Sivjee, G.G., 1992. Airglow Hydroxyl emissions. Planetary and Space Science 40 (23), 235–242.

Sridharan, R., Narayanan, R., Modi, N.K., 1992. An improved chopper mask design for the dayglow photometer. Applied Optics 31, 425–426.

Sridharan, R., Narayanan, R., Pallam Raju, D., 1993. Novel mask design for multiwavelength daytime photometry. Applied Optics 32, 4178–4180.

Sridharan, R., Modi, N.K., Pallam Raju, D., Narayanan, R., Pant, Tarun K., Taori, Alok, Chakrabarty, D., 1998. Multiwavelength daytime photometer — a new tool for the investigations of the atmospheric processes, a new tool for the investigations of the atmospheric processes. Measurement Science and Technology 9, 585–591.

Swenson, G.R., Mende, S.B., Geller, S.P., 1990. Fabry–Perot imaging observations of OH (8,3) rotational temperatures and gravity waves. Journal of Geophysical Research 95, 12,251–12,263.

Takahashi, H., Sahai, Y., Chemesha, B.R., Simonich, D.M., Teixeira, N.R., Lobo, R.M., Eras, A., 1989. Equatorial mesospheric and F-region airglow emissions observed from latitude 4°S. Planetary and Space Science 37 (6), 649–655.

Takahashi, H., Clemasha, B.R., Sahai, Y., Batista, P.R., 1994. Seasonal variations of the mesopause temperature observed at equatorial (4°S) and low (23°S) latitude stations. Advances in Space Research 14 (9), 97–100.

Von Zahn, U., Hoffner, J., Eska, V., Alpers, M., 1996. The mesopause altitude: only two distinctive levels worldwide. Geophysical Research Letters 23, 3231–3234.